https://doi.org/10.1016/j.ultras.2017.03.007

Applications of A Nanocomposite-inspired *in-situ* Broadband Ultrasonic Sensor to Acousto-ultrasonics-based Passive and Active Structural Health Monitoring

Menglong Liu[a‡], Zhihui Zeng[a,b,c], Hao Xu[d], Yaozhong Liao[a‡], Limin Zhou[a], Zhong Zhang[b] and Zhongqing Su[a*]

[a] Department of Mechanical Engineering
The Hong Kong Polytechnic University, Kowloon, Hong Kong SAR

[b] CAS Key Laboratory of Nanosystem and Hierarchical Fabrication
The National Center for Nanoscience and Technology, Beijing 100190, P. R. China

[c] University of Chinese Academy of Science, Beijing 100049, P. R. China

[d] School of Aeronautics and Astronautics, Faculty of Vehicle Engineering and Mechanics, State Key Laboratory of Structural Analysis for Industrial Equipment, Dalian University of Technology, Dalian, 116024, P. R. China

Submitted to *Ultrasonics*

(initially submitted on 25 October 2016; revised and re-submitted on 20 January 2017; further revised and re-submitted on 17 February 2017)

[‡] PhD students

[*] To whom correspondence should be addressed. Tel.: +852-2766-7818, Fax: +852-2365-4703, Email: Zhongqing.Su@polyu.edu.hk (Prof. Zhongqing SU, *Ph.D.*)

Abstract

A novel nanocomposite-inspired *in-situ* broadband ultrasonic sensor previously developed, with carbon black as the nanofiller and polyvinylidene fluoride as the matrix, was networked for acousto-ultrasonic wave-based passive and active structural health monitoring (SHM). Being lightweight and small, this kind of sensor was proven to be capable of perceiving strain perturbation in virtue of the tunneling effect in the formed nanofiller conductive network when acousto-ultrasonic waves traverse the sensor. Proof-of-concept validation was implemented, to examine the sensor performance in responding to acousto-ultrasonic waves in a broad frequency regime: from acoustic emission (AE) of lower frequencies to guided ultrasonic waves (GUWs) of higher frequencies. Results have demonstrated the high fidelity, ultrafast response and high sensitivity of the sensor to acousto-ultrasonic waves up to 400 kHz yet with an ultra-low magnitude (of the order of micro-strain). The sensor is proven to possess sensitivity and accuracy comparable with commercial piezoelectric ultrasonic transducers, whereas with greater flexibility in accommodating curved structural surfaces. Application paradigms of using the sensor for damage evaluation have spotlighted the capability of the sensor in compromising "sensing cost" with "sensing effectiveness" for passive AE- or active GUW-based SHM.

Keywords: ultrasonic sensor; acousto-ultrasonics; nanocomposite sensor; guided ultrasonic waves; acoustic emission; structural health monitoring

1. Introduction

Acousto-ultrasonics, a coalescence of acoustic emission (AE) and ultrasonic characterization [1, 2], has been a subject of intense scrutiny over the years and is now on the verge of maturity for real-world engineering applications. It has gained prominence for developing diverse structural health monitoring (SHM) approaches [3-11] in the past decade, and central to the increased preference of using acousto-ultrasonics lies preliminarily in the fact that it exploits the merits from both AE and guided ultrasonic waves (GUWs) in a broad frequency regime, enabling monitoring at multi-scale so as to accommodate different demands. Acousto-ultrasonics is demonstrably cost-effective in striking a compromise among resolution, detectability, practicality and cost, corroborating the philosophy of *in-situ* SHM.

As a highly sophisticated technique, acousto-ultrasonics-based SHM relies heavily on integrated sensor networks, real-time digital signal processing and pattern recognition – a feature that distinguishes it from conventional non-destructive evaluation. In particular, "sensing", via a sensor network, plays the most rudimentary yet critical role, to collect ambient information and system parameters, whereby a perception on the health status of an inspected structure can be developed. The sensors to serve acousto-ultrasonics-based SHM have been explored extensively [8, 12-21], as typified by piezoelectric wafer active sensors (PWAS) [8, 22], SMART Layer® [17], polyvinylidene fluoride (PVDF)-based interdigital transducers (IDTs) [16], macro fiber composites (MFCs) [18], and circular sensing ring [19] to name a few. In common practice, a limited number of sensors are spatially distributed and networked, to meet a minimal threshold guaranteeing the adequacy of information. During network configuration, a paramount target is to balance "sensing cost" with "sensing effectiveness" – to acquire adequate information with the least weight/volume penalty to the inspected structure. However, owing to its distributed nature, a distributed sensor network may "overlook" certain information, leading to inaccurate or even erroneous results. This has entailed continued efforts to attempt new breeds of sensors for acousto-ultrasonics-based SHM, in lieu of the conventional types of sensor.

Remarkable advances and technological breakthroughs in nanotechnology, materials science, manufacturing and electronic packaging have ushered in a new avenue to develop novel sensors that are inspired by nanocomposites [23-39]. Using a variety of nanofillers such as carbon black (CB) [28, 40], carbon fiber (CF) [41, 42], carbon nanotube (CNT) [31-33] or graphene [43, 44], a nanocomposite sensor can be endowed with merits such as low density, excellent flexibility, easy tailorability in shape and size, chemical stability, low fabrication cost, along with good electrical and mechanical performance. The use of nanocomposite sensors can now be found in a wide application domain, exemplarily including damage identification [23-26], strain measure [27-37, 43, 44] and gas leak detection [38-40, 45, 46].

Nevertheless, the development and use of nanocomposite sensors for acousto-ultrasonics-based SHM is fairly lacking, because of the bottleneck that most nanocomposite sensors may have: the measurand – the change in electrical conductivity of the nanofiller-formed conductive network – is a global indicator with a uniform value between a pair of electrodes, and it reflects only the holistic alteration in material properties right underneath the sensor patch. Limited by this, this type of sensor is unable to respond to damage away from the sensor, and distinguish different locations and degrees of severity of damage. In addition, in order to perceive damage-induced change reliably, especially the ultralow strain magnitude (of the order of micro-strain) in an ultrasonic frequency regime, the sensitivity (gauge factor) of the nanocomposite sensors is to be improved.

In an earlier study [28], the authors have developed and fabricated a novel nanocomposite sensor (made of CB and PVDF). Proven the first of nanocomposite sensor capable of perceiving ultrasonic signals, the developed sensor sees the potential of being applied to acousto-ultrasonic-based SHM. Compared with single-phase rigid ceramic sensor (*e.g.*, lead zirconate titanate (PZT)), the developed nanocomposite sensors, being flexible and lightweight, shows more adaptability to curved structures with a possibility of dense sensor deployment. And compared with metallic foil-based strain gauges, the developed nanocomposite sensor offers a higher gauge factor [28] and therefore greater sensitivity to structural or ambient changes and higher possibility of sensing faint elastic disturbance induced by acousto-ultrasonics. Nevertheless, the quantitative evaluation of the sensing performance of the developed sensor for its applications to SHM has yet been fully demonstrated. Relevant issues associated with the application, including parameter setup, sensor networking, measurement system configuration, algorithm development, etc., are to be explored.

In recognition of the stated deficiencies of nanocomposite sensors when they are attempted to accommodate acousto-ultrasonics-based SHM, this study is dedicated to the quantitative experimental validation of the developed nanocomposite-inspired broadband ultrasonic sensor, capable of responding to acousto-ultrasonic waves (embracing AE and GUWs) faithfully and accurately, either in a passive or active manner. Through constituent optimization, the developed sensor is proven quantitatively responsive to GUWs up to 400 kHz. Lightweight and small, the sensor is demonstrated to surpass conventional ultrasonic transducers such as PZT in some aspects, including the possibility to coat on a structure and flexibility adapt to a curved structural surface, with reduced use of wiring and cabling. To take a step further, the developed sensors are networked to form a dense sensor network, well addressing an *in-situ* sensing philosophy and showing recommendable capability in balancing “sensing cost” with “sensing effectiveness”.

This paper is organized as follows. Section 2 briefly introduces the development, fabrication and optimization of the nanocomposite sensor. In this section, the sensing mechanism of the sensor in responding to acousto-ultrasonic waves, based on the tunneling effect in the formed nanofiller conductive network, is explained and validated via material morphological characterization tests. Section 3 concerns the conformance tests of the developed sensor, in a broadband regime. For calibration, signals measured with the nanocomposite sensor are compared with those obtained with conventional PZT wafers. Upon conformance validation, the developed sensor is applied to damage identification paradigms including impact localization (using low-frequency AE waves in a passive manner) and quantitative damage evaluation (using high-frequency GUWs in an active way), as detailed in Section 4, followed with concluding remarks in Section 5.

2. Sensor Fabrication and Characterization

Targeting a broad range of response, the nanofiller and matrix of the nanocomposite sensor were selected prudently according to twofold consideration: (i) the time- and frequency-dependent viscoelastic properties of the candidate materials should be minute, facilitating the sensor to be responsive to broadband acousto-ultrasonic waves from low-frequency AE waves to high-frequency GUWs; and (ii) the gauge factor should be sufficiently high, endowing the sensor with a capability to perceive GUWs of ultralow magnitudes. A variety of nanofillers, including CB and CNT of various aspect ratios, has been attempted, among which CB was selected as the nanofiller, owing to its lower aspect ratio and therefore a higher specific surface and less amount of nanoparticle entanglement, compared with other candidate CNT nanofillers. This attribute of CB is beneficial to the formation of an even, stable and uniform conductive network in the sensor, to enhance the sensitivity of sensor to broadband acousto-ultrasonic waves. On the other hand, PVDF was chosen as the matrix, on the grounds that PVDF is a thermoplastic material with advantages including easy-processing, extreme flexibility, low density, chemical inertness, thermal stability, and good mechanical performance [29, 30, 47]. With a higher elastic modulus, PVDF shows a faster response than rubber-based piezoresistive materials (rubber-based matrix candidates often exhibit complex time- and frequency-dependent viscoelastic properties, unwieldy to respond to dynamic loads).

Nanocomposite films were fabricated according to the process detailed in [28]. As shown in Figure 1 (a), the film shows good resilience, highlighting its potential to adapt to a curved structural surface. To further fabricate a nanocomposite film into a functional sensor for acquisition of acousto-ultrasonic waves, the developed films were tailored to individual rectangular flakes (10 mm × 8 mm, thickness remained at ~200 μm). Silver conductive adhesive (D05001, Beijing Emerging Technology Co. Ltd., China) was pasted on each flake, leading to two electrodes to which shielded cables were glued, as shown in Figure 1 (b). It is noteworthy that the nanocomposite material between the two electrodes is the sensor *per se*, in which the formed conductive network is responsive to GUWs. Lightweight and flexible, each sensor, in a modality of thin film, can be produced via a standard fabrication process, and deployed in a large quantity to configure a sensor network for acquisition of acousto-ultrasonic waves. Repeating the above process, a series of nanocomposite sensor featuring various weight ratios of CB to PVDF, ranging from 5 to 30 wt%, were prepared in a comparative manner.

(a)

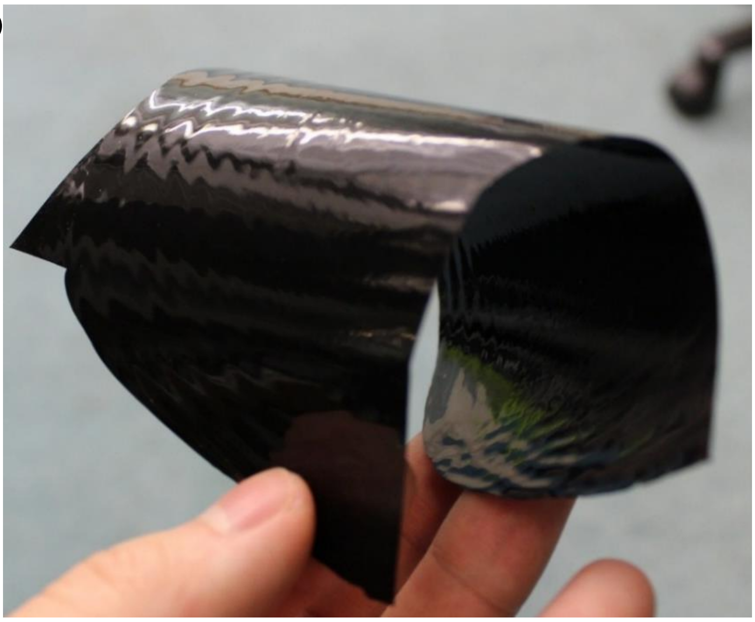

(b)

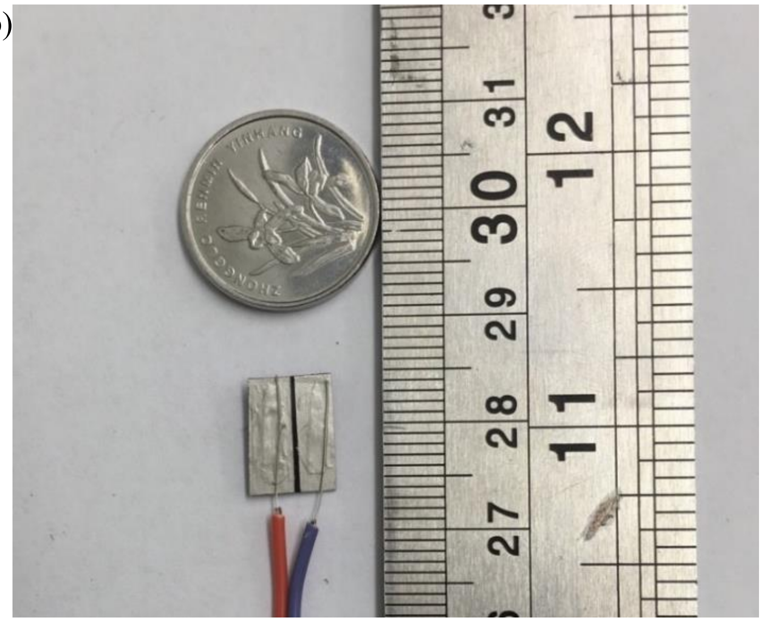

Figure 1 (a) A prepared nanocomposite film, showing good resilience; (b) a developed sensor with silver-pasted electrodes and shielded cables

To determine an optimal nano-structure of the sensor so as to enhance its sensing sensitivity, a series of material characterization tests on the developed nanocomposites was implemented. Electrical conductivity (σ) of the nanocomposite films with five representative weight ratios of CB nanofiller (i.e., 5, 6.5, 8, 20 and 30 wt%, respectively) was measured [28], which has affirmed that 6.5 wt% was the percolation threshold of the CB conductive network. Percolation threshold represents a critical transition of the nanocomposites from insulation to conduction, at which the nanocomposites exhibit the highest sensitivity to external disturbance (e.g., the strain induced by acousto-ultrasonic waves). Figure 2 (a) displays the scanning electron microscopy (SEM) (JSM-7500F, JEOL Ltd) image of the nanocomposites (with ~6.5 wt% of CB nanofiller), revealing even and uniform dispersion of nanoparticles in matrix PVDF.

Upon determination of the percolation threshold, electro-mechanical properties of the nanocomposites with 6.5 wt% of CB nanofillers were examined, using a semi-conductor characterization system (4200-SCS, Keithley Instruments, Inc.) installed on a dynamic mechanical testing platform (TA Q800, TA Instruments). σ of the nanocomposite films was measured using a two-probe method when the films were subjected to a quasi-static (1/120 Hz) cyclic tensile load until a maximum strain of 1% was reached (with a strain ramp rate of 0.5%/min). Figure 2 (b) shows the obtained response of the nanocomposite films against the cyclic load, to observe superb consistency between the response of the nanocomposite films and the applied load, without observable hysteresis and distortion in response waveform.

(a)

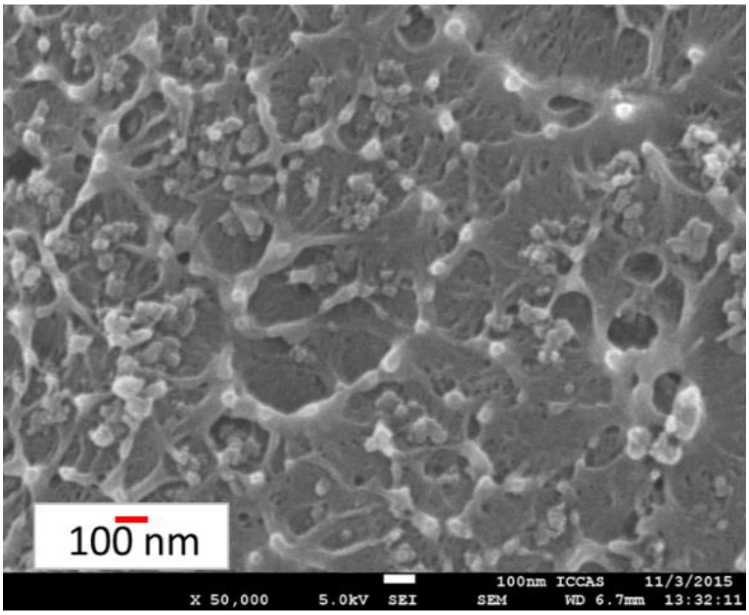

(b)

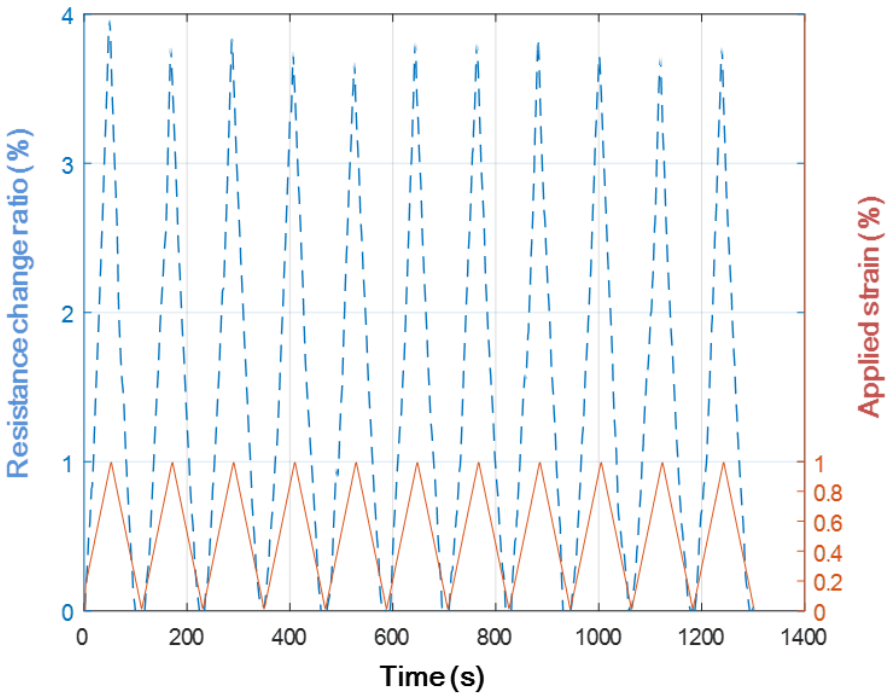

Figure 2 (a) SEM image of nanocomposites with ~6.5 wt% of CB nanofillers; and (b) electro-mechanical response of prepared CB/PVDF nanocomposites (6.5 wt% of CB nanofillers) subjected to a quasi-static load (1/120 Hz)

To extend the above examination from a quasi-static (1/120 Hz) frequency to higher frequencies, a developed nanocomposite film sensor (6.5 wt% of CB nanofillers) was surface-bonded on a glass fiber/epoxy composite beam (290 mm long, 38 mm wide and 2 mm thick), as shown in Figure 3 (a). The beam was excited 270 mm from the clamped end via an electro-mechanical shaker (B&K® 4809) with a sinusoidal signal of 2000 Hz. For the purpose of calibration and comparison, a commercially available metal-foil strain gauge (with a gauge factor of ~2) was collocated aside the nanocomposite sensor, both having the same distance of 200 mm to the excitation point.

The magnitude of an acousto-ultrasonic wave can be faint, particularly when it is in a frequency range of kilo- or mega-Hertz – that is the case for GUWs used for acousto-ultrasonics-based SHM, in which the magnitude of the GUW-induced strain is usually of several micro-strains only. With such a low degree of magnitude, a captured acousto-ultrasonic wave signal can be naturally prone to contamination from environment noise and measurement uncertainties, leading to a low signal-to-noise ratio. To this end, a self-developed signal amplification module was configured, to be used in conjunction with the sensor. The signal amplification module mainly integrates a Wheatstone bridge with adjustable resistors compatible with the electrical resistance of the nanocomposite sensor, an electronic amplifier circuit, a series of high-pass and low-pass filters and a signal conversion circuit for converting measured piezoresistivity to electrical signals.

Using an oscilloscope (Agilent® DSO9064A), acousto-ultrasonic wave signals acquired with both the nanocomposite sensor and strain gauge were registered, with an example displayed in Figure 3 (b). Both signals show high consistency, as well as good reversibility and repeatability of measurement. Observation from this electro-mechanical test argues that the fabricated sensor made with CB/PVDF nanocomposites at its percolation threshold (~6.5 wt% of CB nanofillers) is responsive to a dynamic excitation up to 2000 Hz, without observable hysteresis and deviation in response waveform and with a greater gauge factor (~10) five times larger than conventional strain gauges (~2). It is noteworthy that the gauge factor increases as the sensing frequency (~4 in the quasi-static cyclic loading of 1/120 Hz and ~10 in the vibration test of 2000 Hz), which facilitates the application of the developed CB/PVDF sensor for perception of acousto-ultrasonic waves.

(a)

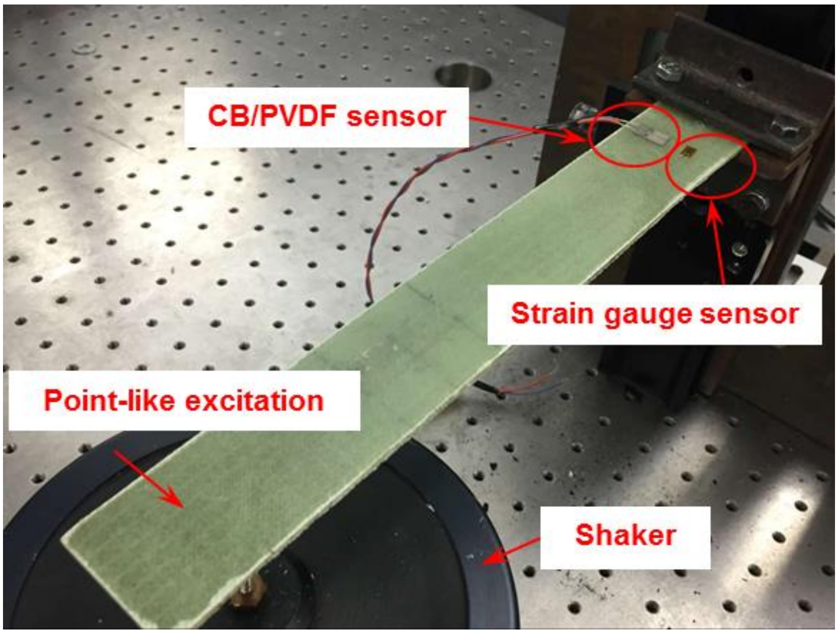

(b)

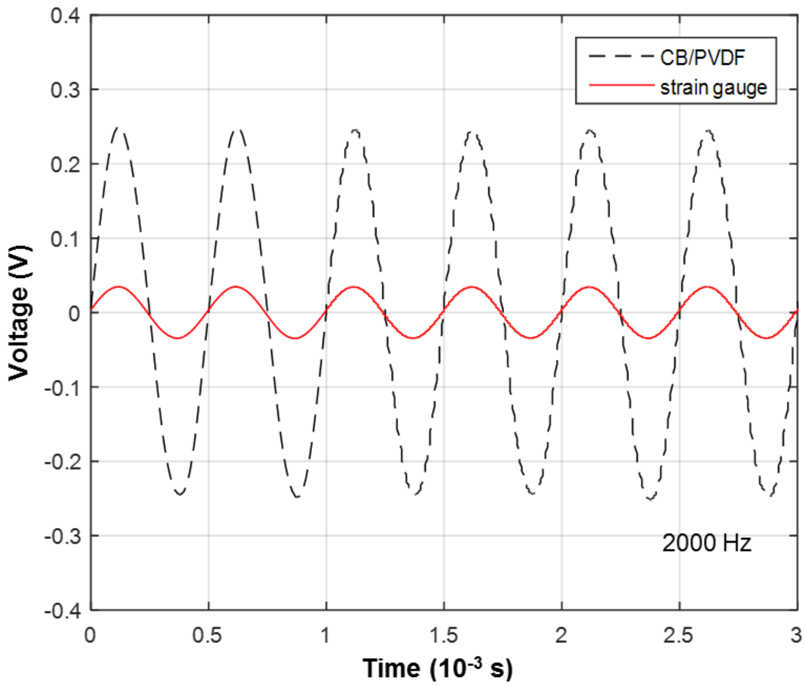

Figure 3 (a) Experiment set-up for acquisition of vibration signal of a glass fiber/epoxy composite beam using the prepared nanocomposite sensor (6.5 wt% of CB nanofillers); and (b) comparison of signals captured with nanocomposite sensor and metal-foil strain gauge (at 2000 Hz)

To achieve insight into the sensing mechanism of the developed nanocomposite sensor in responding to broadband acousto-ultrasonic waves, an X-ray diffraction (XRD) test [28] was accomplished, to confirm that the prepared CB/PVDF nanocomposites feature a pattern of α-crystal with a non-polar crystal structure. This suggests that the piezoresistivity manifested by the developed sensor is from the change in nanofiller-formed conductive network caused when an acousto-ultrasonic wave traverses the sensor, rather than from the piezoelectricity effect of PVDF matrix itself. This is because only a polar crystal (such as a β-crystal) can lead to piezoelectricity (as interpreted elsewhere [35]). Based on XRD results, conclusion can be drawn that the predominant sensing mechanism of the developed nanocomposite sensor is the tunneling effect [31-33] present in the conductive network formed by CB nanoparticles (as well as their aggregations) when the sensor is exposed to an acousto-ultrasonic wave. In brief, the tunneling effect, at nanoscale, occurs when neighboring nanoparticles are in a close proximity (normally several nanometers) but not in a direct contact. When the sensor (at the determined percolation threshold) is subjected to an acousto-ultrasonic wave, the distances among adjacent nanoparticles alter, leading to the tunneling effect of charged carriers. As a direct consequence of the tunneling effect, the conductivity of the nanofiller network and consequently the electrical resistance measured by the sensor varies – that is the primary sensing mechanism of the sensor in responding to broadband acousto-ultrasonic waves.

3. Sensor Calibration for Acquisition of Acousto-ultrasonic Waves

Upon determination of an optimal nano-structure, the developed CB/PVDF nanocomposite film sensor was calibrated for *in-situ* perception of acousto-ultrasonic waves ranging from low-velocity-impact-induced low-frequency AE waves to active high-frequency GUWs.

3.1. Experiment Set-up

A glass fiber/epoxy composite panel (600 mm × 600 mm × 2 mm) was prepared with its four edges clamped, to which a fabricated nanocomposite sensor (denoted by CB_1 hereinafter) and two commercial PZT wafers (Physik Instrumente Co., Ltd., PIC151; 9 mm in diameter and 0.5 mm in thickness; denoted by PZT_1 and PZT_2) were surface-mounted with an instant glue, shown schematically in Figure 4. PZT_1, centralized on the panel with a distance of 150 mm to the nanocomposite sensor, was used to capture low-frequency AE signals in a passive drop test (Section 3.2) or to generate high-frequency GUWs in an active GUW test (Section 3.3), while PZT_2, 100 mm from PZT_1, functioned as a sensor to acquire active GUWs generated by PZT_1 (in Section 3.3).

Due to different sensing philosophies of these two types of sensor (piezoelectric effect for PZT wafer, while tunneling effect-induced piezoresistive effect for nanocomposite sensor as interpreted in Section 2), different signal acquisition methods were adopted: PZT wafers were instrumented with an oscilloscope (Agilent® DSO9064A), while CB/PVDF with the self-developed test system as detailed in Section 2.

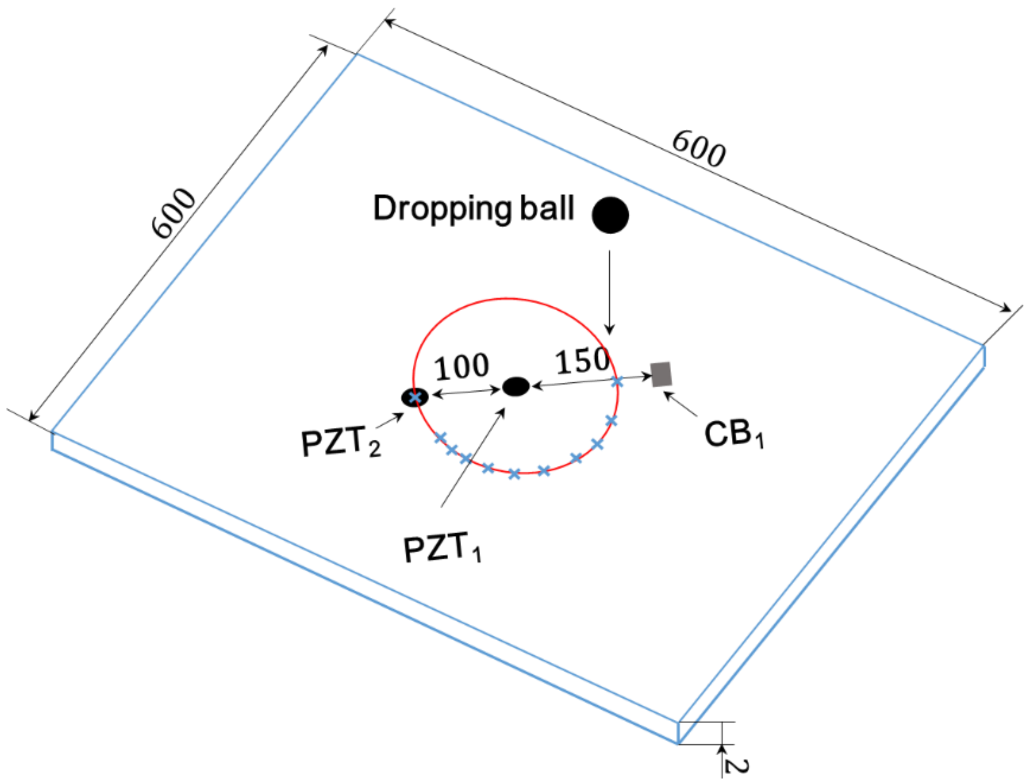

Figure 4 Schematic of experimental set-up for *in-situ* perception of acousto-ultrasonic waves (unit: mm)

3.2. Acquisition of Low-frequency AE Signals

A drop test was performed using the experimental set-up in Figure 4, in which a steel ball (8 mm in diameter) impinged on the panel from a height of 300 mm to introduce an impact energy of ~6.3×10^{-3} J to the panel. The generated AE waves were then captured with both sensors (CB_1 and PZT_1) at a sampling rate of 1 MHz. The drop test was repeated, introducing impact energy to the panel at different spots along the periphery of a circle with a radius of 100 mm and PZT_1 being the center (symbol "×" in Figure 4), this leading to different distances from the impact spot to the nanocomposite sensor, varying from 50 to 250 mm.

A set of typical AE signals acquired with PZT_1 and CB_1, at a respective distance of 100 mm and 90 mm to the impact spot, is shown in Figure 5 (a). To mitigate measurement noise, all raw signals were processed with a first-order Butterworth low-pass filter with a cutoff frequency of 10 kHz, and the accordingly processed signals are presented in Figure 5 (b), to observe a good coincidence in performance between the nanocomposite sensor and the PZT wafer. The zeroth order anti-symmetric mode (A_0) is observed to be the dominant propagating wave mode in the low-velocity-impact-induced AE signals. Further, Figure 6 compares the spectra of the two signals in Figure 5, affirming that the nanocomposite sensor responds to a signal of a frequency as high as 5 kHz, with comparable performance with commercial PZT-type sensors.

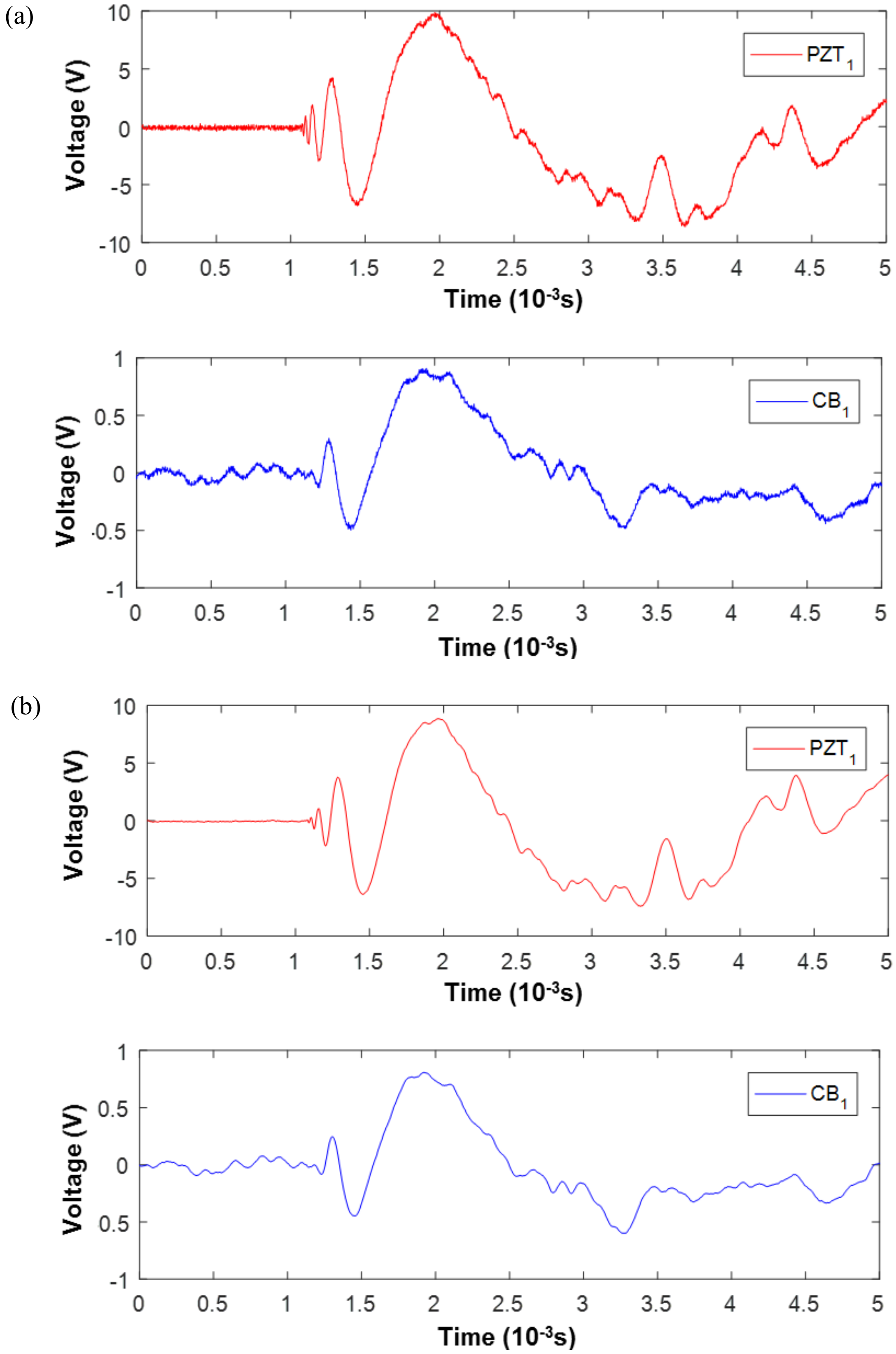

Figure 5 (a) Raw and (b) noise-filtered AE wave signals acquired with PZT_1 and CB_1 at a respective distance of 100 mm and 90 mm to the impact spot

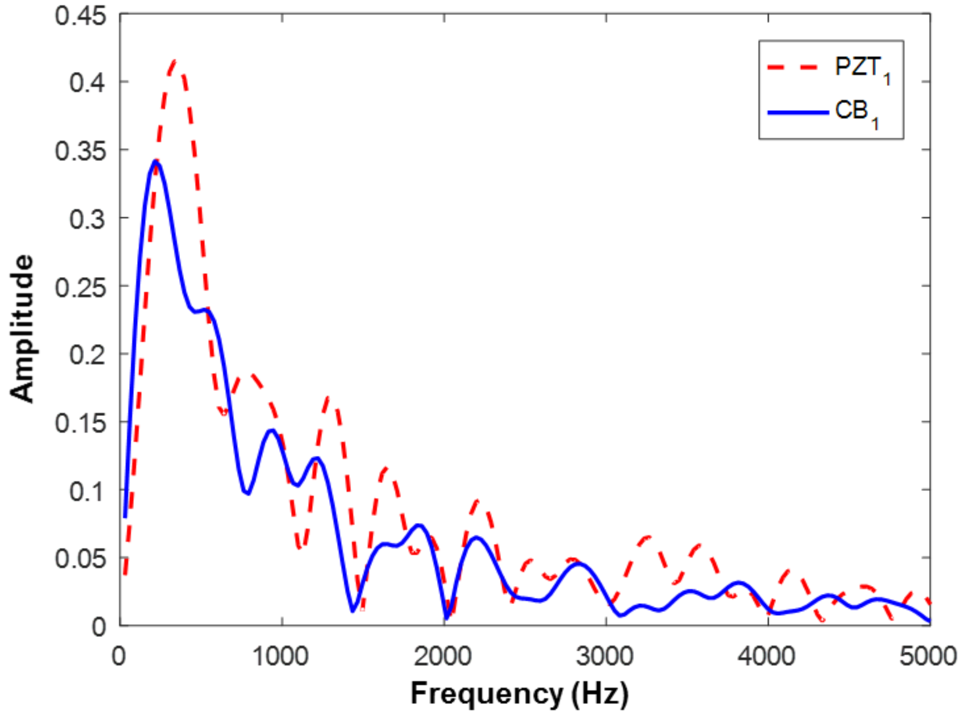

Figure 6 Comparison of spectra of signals in Figure 5 acquired with PZT_1 and CB_1

3.3. Acquisition of High-frequency GUW Signals

GUWs in an ultrasonic regime feature extremely low strains (of the order of micro-strain) whereas ultrafast dynamic change (>20 kHz). The acquisition of high-frequency GUW signals using the developed nanocomposite sensor was validated, with the panel in Figure 4. The GUW generation and acquisition system includes a waveform generator (NI® PXI-5412 integrated in the NI® PXIE-1071 4-slot chassis), a linear power amplifier (Ciprian® US-TXP-3), and the self-developed signal amplification and acquisition module as detailed in Section 2. In the test, the wave generator output five-cycle Hanning-windowed sinusoidal tone-bursts at central frequencies from 50 kHz to 400 kHz. Upon amplification to 400 Vp-p to the linear power amplifier, the tone-bursts excited PZT_1 to produce GUWs propagating in the panel, which were then acquired with CB_1 and PZT_2, respectively, at a sampling rate of 20 MHz. Notably, in order to eliminate possible interference from the PZT on the nanocomposite sensor, different wave propagation distances were set deliberately to two types of sensor: 100 mm from PZT_1 to PZT_2, and 150 mm from PZT_1 to CB_1.

At a representative frequency of 200 kHz, the excitation signal and accordingly acquired GUW signals with CB_1 and PZT_2 are shown in Figure 7. The raw signal acquired with CB_1, Figure 7 (a), is noted to embrace the zeroth order symmetric Lamb wave mode (S_0) – the first-arrival wave component, and a high-voltage (400 Vp-p) crosstalk induced by the linear power amplifier. Owing to distinct sensing mechanisms – the piezoelectric effect for PZT and piezoresistive effect for CB/PVDF – the signal acquired with PZT shows a higher magnitude and higher signal-to-noise ratio. Upon applied with a Butterworth filter (Figure 7 (b)) and a Hilbert transform (Figure 7 (c)), both signals become more explicit and consistent, to observe good and quantitative agreement in between, in terms of the waveform and arrival moment of the concerned wave mode. The filtered signals were then used for damage detection.

(a)

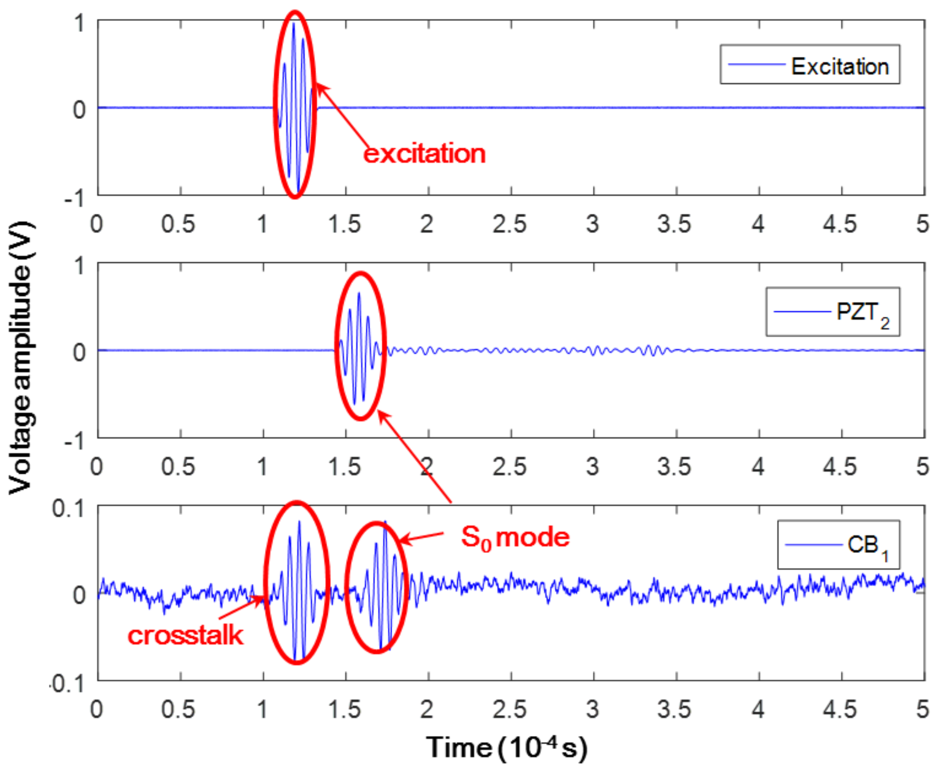

(b)

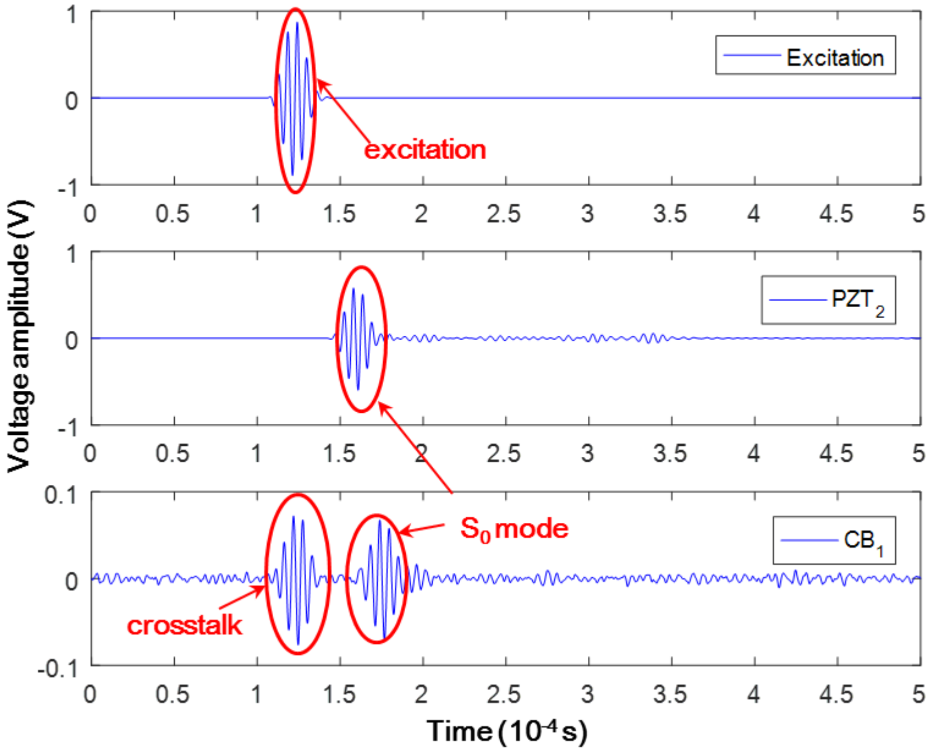

(c)

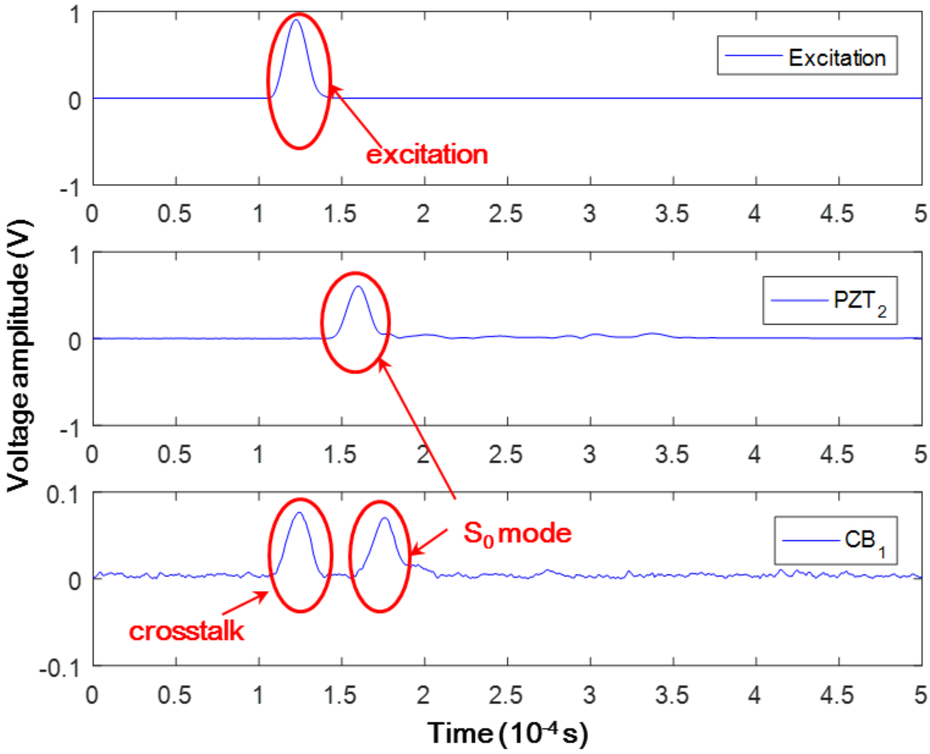

Figure 7 (a) Raw GUW signals captured with PZT_2 and CB_1 at 200 kHz; (b) filtered signals using Butterworth filter; and (c) processed signals using Hilbert transform (Note: the arrival time of S_0 mode in PZT_2- and CB_1-captured signals is different because of the different distances from PZT_1 to PZT_2 and to CB_1)

To extend the above discussion (at 200 kHz), a series of tone-bursts from 50 kHz to 400 kHz was excited via PZT_1, and Figure 8 (a) displays the normalized magnitudes of the signals acquired by PZT_2 and CB_1, respectively. The nanocomposite sensor is observed to reach a response peak at 175 kHz within the discussed frequency range, compared with PZT at 250 kHz – a property knows as “mode tuning” (i.e., the magnitude of the sensor response varies subjected to excitation frequency) [11, 48]. The difference in mode tunning between two sensors (175 kHz for nanocomposites while 250 kHz for PZT) could be attributed to the different sensing mechanisms of nanocomposite sensor and PZT.

With GUW signals in Figure 8 (a), Figure 8 (b) further compares the ascertained propagation velocities of S_0 and A_0 at various excitation frequencies, to note a coincident performance of two types of sensor in responding to various GUW mode in a wide frequency range as high as 400 kHz, with a weak magnitude as low as ~ 10 micro-strain. This has testified the superior capacity of the developed nanocomposite sensor as a broadband ultrasonic sensor.

(a)

(b)

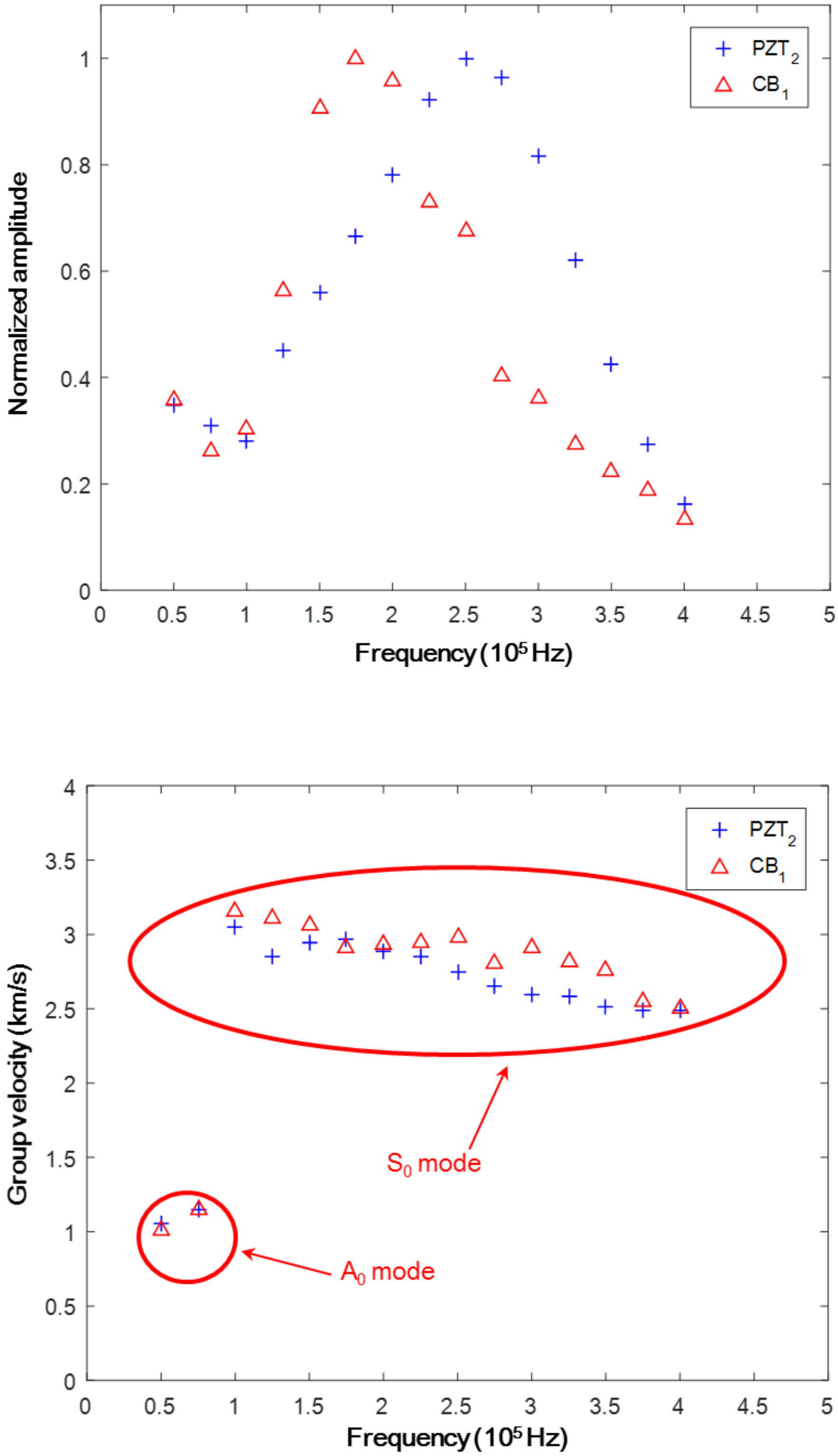

Figure 8 Variation in response of prepared CB/PVDF nanocomposite sensor (6.5 wt% of CB nanofillers) to excitation, compared with PZT: (a) normalized magnitude *vs.* excitation frequency; (b) group velocity *vs.* excitation frequency

4. Applications to Passive and Active Damage Characterization

Upon material characterization, optimization, performance calibration and conformance tests, the developed CB/PVDF nanocomposite film sensor was applied to two paradigms of damage characterization – passive impact localization and active damage identification. In both paradigms, the sensor performed as a broadband ultrasonic sensor for *in-situ* acquisition of acousto-ultrasonic waves. In addition, being lightweight and flexible, individual film sensors were networked in a dense fashion, to render rich information for depicting damage with desirable redundancy and hence enhanced reliability of signal acquisition, outperforming traditional piezoelectric counterpart in terms of adaptability to complex structure and information redundancy. With the sensor network, damage was evaluated quantitatively with parameters including presence, location and severity.

4.1. Passive Paradigm: Impact Localization

Eight nanocomposite sensors (denoted by CB_1~CB_8) were surface-glued on an all-boundary-clamped fiber-epoxy composite plate, see Figure 9, to form a sensing network with an inspection coverage of approximately 300 mm × 300 mm. A drop test with the same configuration used earlier (Section 3.1), including the same degree of impact energy, was recalled. In the test, a steel ball impinged on the plate at eight locations, as marked with symbol “cross” (×) in Figure 9 (b), each of which had the same distance of 100 mm to a PZT wafer centralized on the plate (denoted by PZT_1). The procedure and configuration of signal acquisition were remained the same as those used in Section 3.1.

(a)

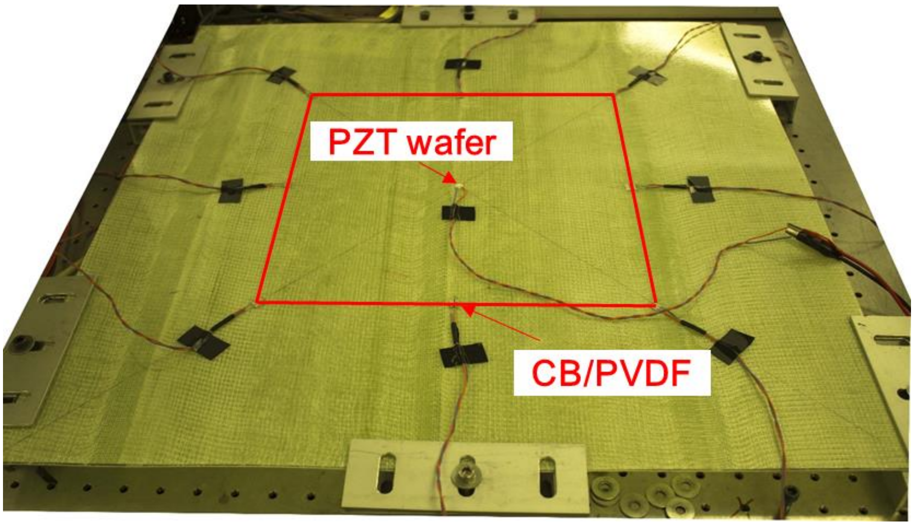

(b)

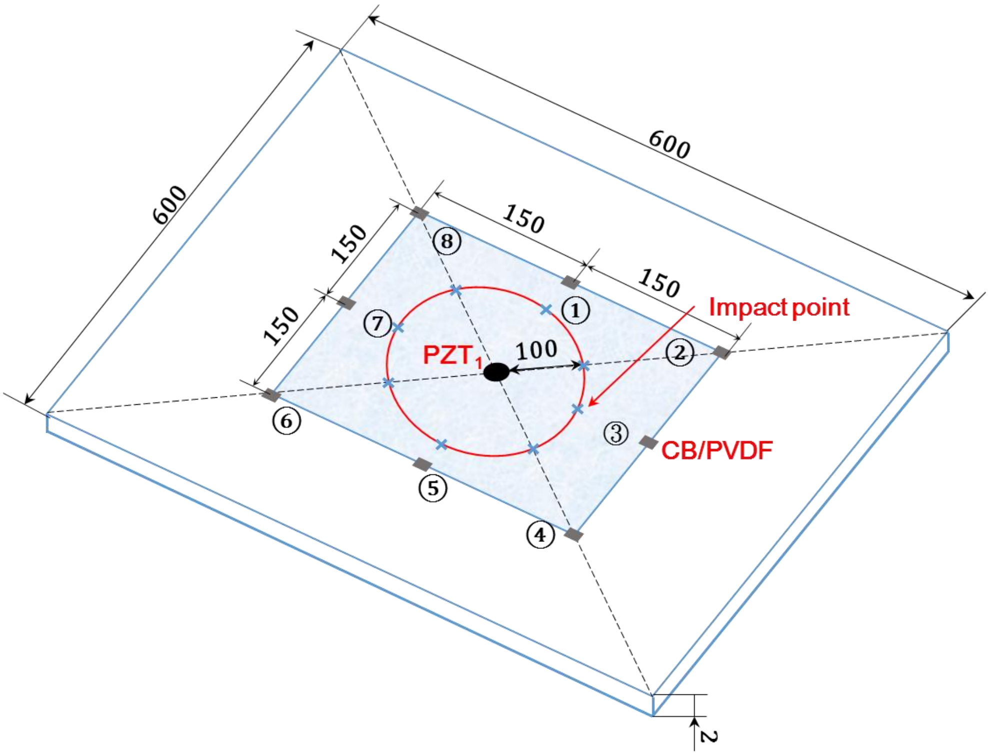

Figure 9 (a) Photographed and (b) schematic description of experimental set-up (with a surface-glued sensor network formed by nanocomposite film sensors), for passive impact localization and active damage identification (unit: mm)

With obtained AE wave signals, a *delay-and-sum* imaging algorithm [49] was recalled to locate impact spots in eight drop tests. In the algorithm, the first-arrival wave component captured with the i^{th} sensor, located at (x_i, y_i), in the sensor network (denoted by CB_i) is expressed as

$$t_i = t_0 + \Delta t_i , \tag{1}$$

where t_0 is the moment when the steel ball impacts the plate, and Δt_i the subsequent traveling time for A_0 wave mode in the signal from the impact spot to CB_i (it has been earlier demonstrated in Section 3.2 that A_0 mode dominates a low-velocity-impact-induced AE signal).

Taking into account another sensor in the sensor network, say CB_j at (x_j, y_j), and assuming the impact spot is at (x, y) within the inspection coverage, the time difference ($\Delta t_{ij}(x, y)$) in the arrival time of A_0 captured by CB_i and CB_j yields

$$\begin{aligned} \Delta t_{ij}(x, y) &= t_i - t_j = (t_0 + \Delta t_i) - (t_0 + \Delta t_j) \\ &= \frac{\sqrt{(x - x_i)^2 + (y - y_i)^2} - \sqrt{(x - x_j)^2 + (y - y_j)^2}}{v_{plate}}. \end{aligned} \tag{2}$$

In Eq. (2), variables are distinguished by subscripts i and j for two individual sensors. v_{plate} represents the velocity of A_0 mode.

With the sensor pair formed by CB_i and CB_j, a two-dimensional gray-scale image can be synthesized using the *delay-and-sum* algorithm, with its pixel value ($\xi_{ij}(x, y)$) defined as

$$\xi_{ij}(x, y) = \max(E_i + E_j(\Delta t_{ij}(x, y))) , \tag{3}$$

where E is the energy packet of A_0 mode obtained using a wavelet transform. With a compensation for the time delay of $\Delta t_{ij}(x, y)$ in the arrival time of A_0 mode in the signal captured by CB_j, with regard to that in the signal captured by CB_i, the max operator in Eq.

(3) defines the peak value of the summation of two time-series signals acquired with CB_i and CB_j, which is then linked to the probability of existence of impact spot within the inspection coverage – the perceptions as to the impact spot from the perspective of the sensor pair CB_i and CB_j. According to Eqs. (2) and (3), all the pixels in the image which feature the same time delay will form a set of hyperbola, with CB_i and CB_j being its two foci. The hyperbola suggests all the possible locations of impact within the inspection coverage. In principle, those pixels with greater value of $\xi_{ij}(x, y)$ have higher degrees of probability of impact spot therein, and vice versa.

Aggregating images constructed by all available sensor pairs in the sensor network through appropriate image fusion algorithms, a superimposed image can be hypothesized – a collective consensus as to the impact spot from the entire sensor network. Without loss of generality, taking the AE signal acquired with CB_1 as reference, one has, for the current sensor network involving eight nanocomposite sensors,

$$\xi_{sum}(x, y) = \max(\sum_{j=2}^{8}(E_1 + E_j(\Delta t_{1j}(x, y))) . \quad (4)$$

As representative results, Figure 10 (a) and (b) exhibit the identified impact spots in two out of eight drop tests, in which a nonlinear normalization process was applied for enhanced focusing. Figure 10 (c) shows the combined results for all the eight tests. A high degree of coincidence between identified impact spots and reality can be noted, affirming the performance of the developed nanocomposite sensor in passive AE-based damage localization.

(a)

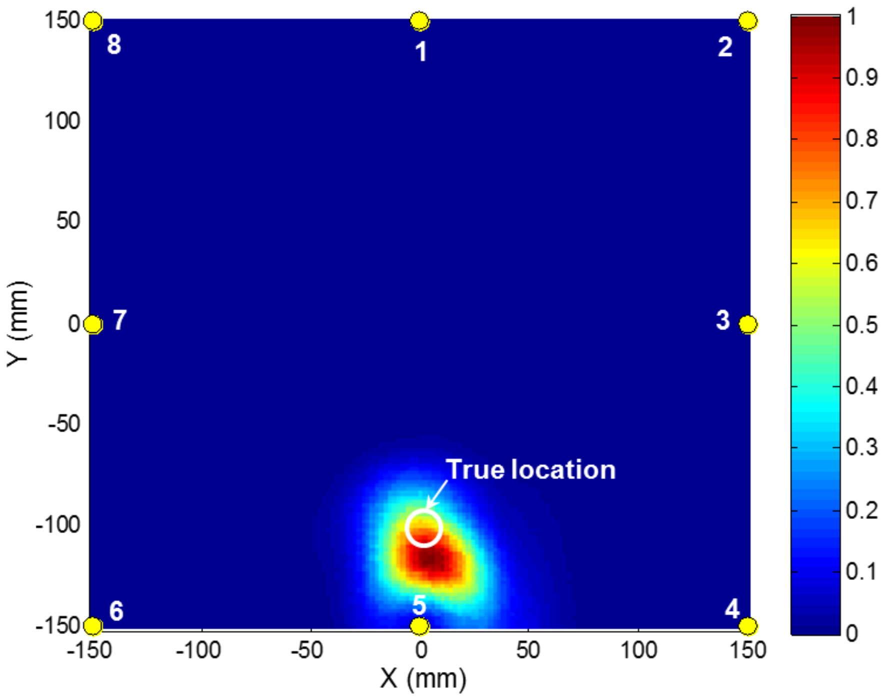
True location
Y (mm)
X (mm)
1
2
3
4
5
6
7
8

(b)

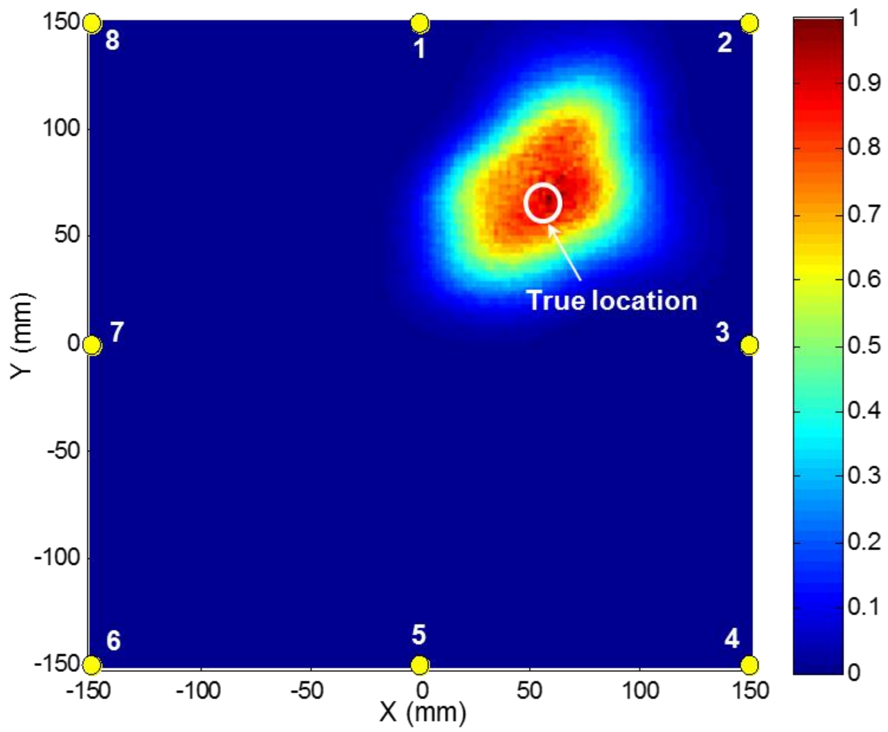
True location
Y (mm)
X (mm)
1
2
3
4
5
6
7
8

(c)

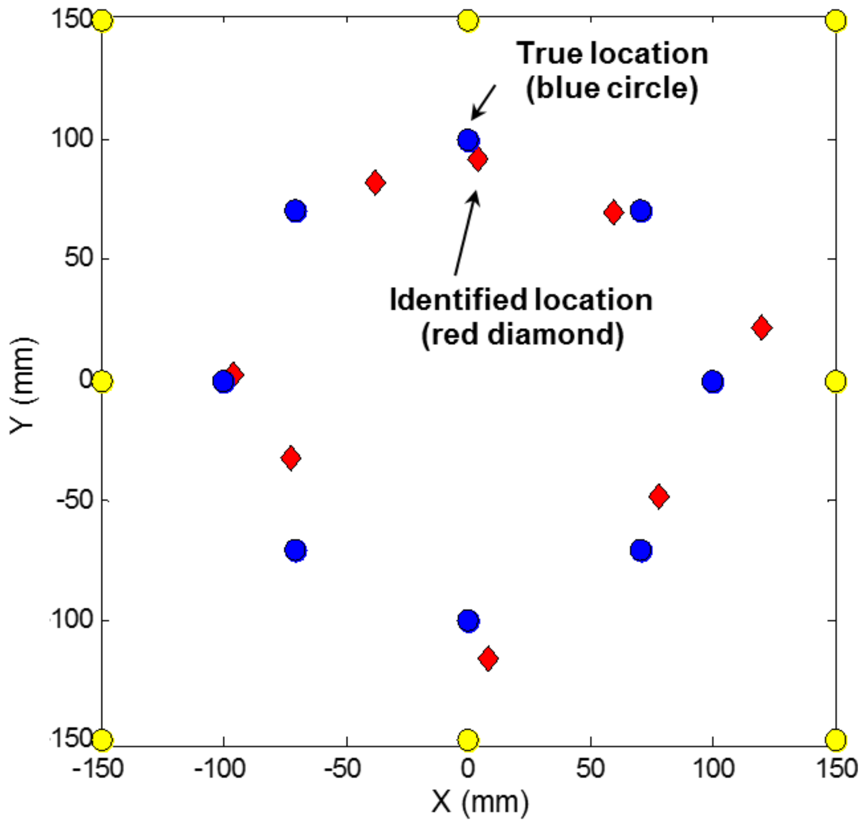

Figure 10 Comparison between identified and real impact spots using impact-induced passive AE signals captured with the nanocomposite sensors, when the real spot is at (a) (0, -100); (b) (71, 71); and (c) combined results for eight drop tests (unit mm)

4.2. Active Paradigm: Quantitative Characterization of Mock-up Damage

Using the same glass fiber-epoxy composite plate in Section 4.1, PZT_1, as a wave generator, produced a five-cycle Hanning-windowed sinusoidal tone-burst at a central frequency of 200 kHz with a magnitude of 400 Vp-p. The selection of 200 kHz lies in the fact that at this frequency, S_0 mode becomes predominant in GUWs, according to the "mode tuning" effect (Section 3.3). It is noteworthy that different sensing mechanisms between the developed nanocomposite sensor and the PZT sensor decide the different "mode tuning" effect, through which 200 kHz was selected to ensure a high signal-to-noise ratio. The propagation velocity of S_0 mode was ascertained in Figure 8. A mock-up damage (simulated using an adhesive tape measuring 20 mm × 20 mm × 3 mm) was introduced to the composite plate. The generated GUWs were acquired with the eight CB/PVDF nanocomposite sensors at a sampling rate of 20 MHz. The *delay-and-sum*-based imaging algorithm, as elaborated in Section 4.1, was applied. As representative results, Figure 11 shows the identification results for two scenarios when the mock-up damage was at (75 mm, 0 mm) and (0 mm, -75 mm), respectively. Though not pinpointing the damage quantitatively and accurately (due to the use of only a few sensors), the identification results are still able to point out the region where the mock-up damage exists. This has substantiated a wide application domain of the developed nanocomposite sensor from passive AE-based impact localization to active GUWs-based quantitative damage characterization.

(a)

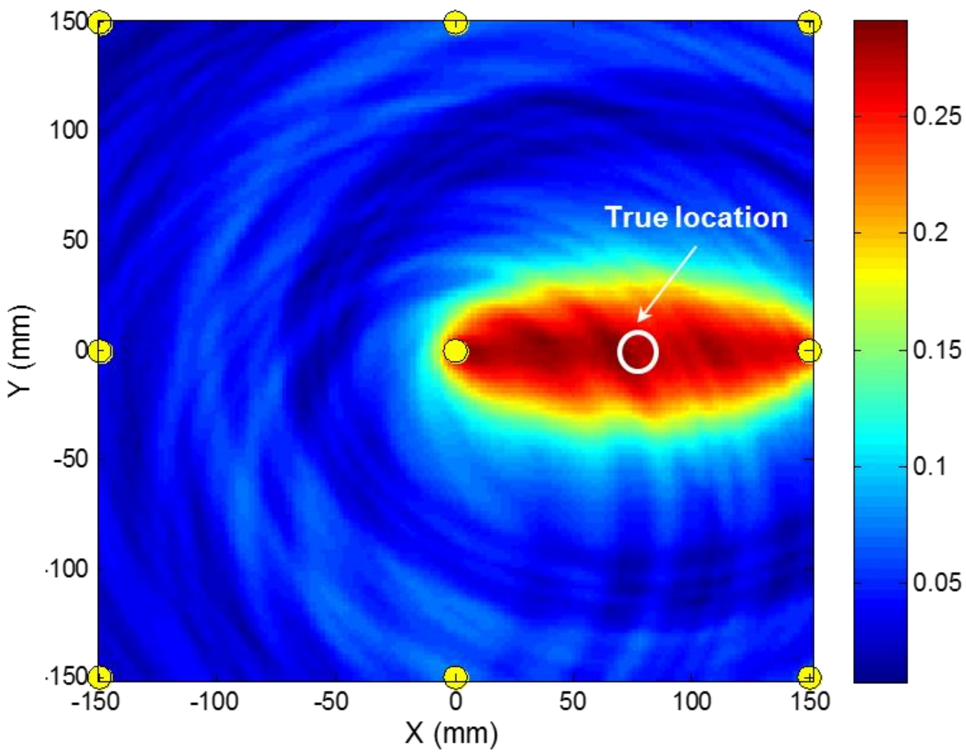

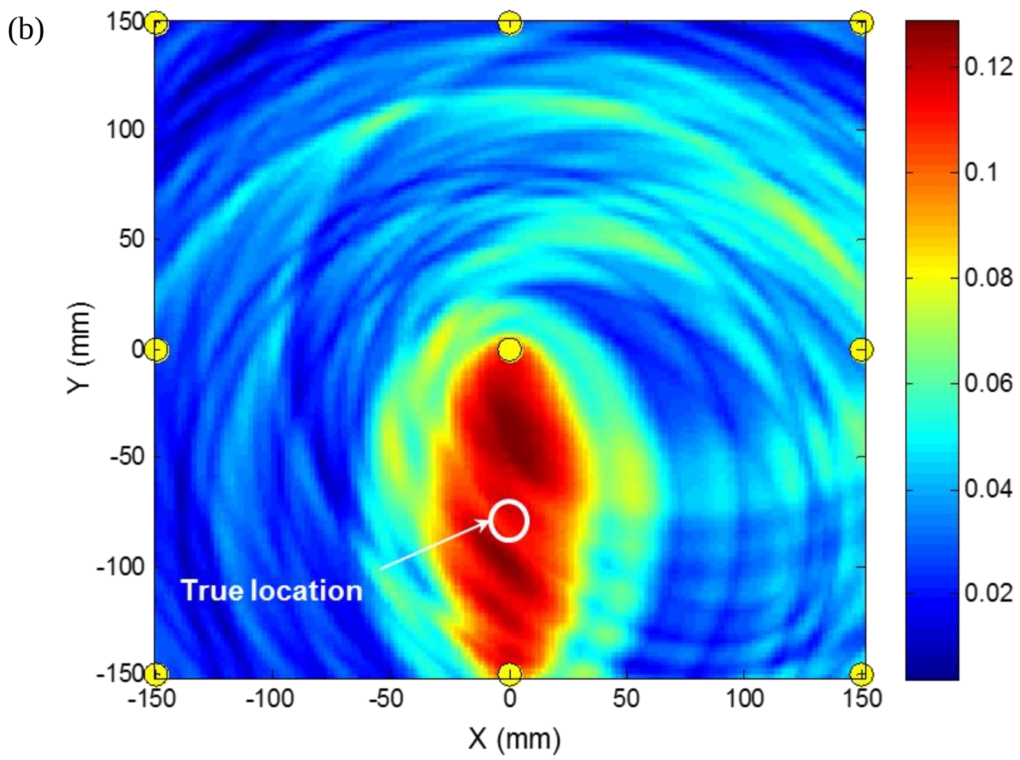

Figure 11 Comparison between identified and real damage using actively generated GUWs captured with the nanocomposite sensors, when the real damage is at (a) (75, 0); and (b) (0, -75) (unit mm)

5. Concluding Remarks

In this study, the previously developed nanocomposite sensors, with the tunneling effect being the dominant sensing mechanism, were networked for implementation of acousto-ultrasonics-based damage characterization. Through the optimization of nano-structure and nanofiller constituent (~6.5 wt%) of the sensor, the sensing performance of the nanocomposite-inspired *in-situ* broadband ultrasonic sensor made of CB/PVDF was validated, and experimentally evaluated quantitatively to perceive broadband response with frequencies up to 400 kHz: from low-frequency vibration (2000 Hz), through impact-induced AE waves (<5 kHz), to GUWs (up to 400 kHz), with high fidelity, ultrafast response and high sensitivity. The sensor presents a much greater gauge factor (~10) under vibration of 2000 Hz compared with conventional metal-foil strain gauge (~2), and greater flexibility in accommodating curved structural surfaces. Lightweight, flexible, coatable to a structure and deployable in a large quantity to form a dense sensor network for *in-situ* acquisition of acousto-ultrasonic waves in either a passive or active manner, this new type of broadband ultrasonic sensor has unfolded its application prospect towards acousto-ultrasonics-based SHM.

Acknowledgements

This project is supported by the Hong Kong Research Grants Council via General Research Fund (No. 15214414 and No. 15201416).

References

[1] T. Kundu, Acoustic source localization, Ultrasonics, 54 (2014) 25-38.

[2] J.L. Rose, Ultrasonic guided waves in solid media, Cambridge University Press, 2014.

[3] N. Quaegebeur, P. Masson, P. Micheau, N. Mrad, Broadband generation of ultrasonic guided waves using piezoceramics and sub-band decomposition, IEEE T. Ultrason. Ferr., 59 (2012) 928-938.

[4] H. Huang, D. Paramo, Broadband electrical impedance matching for piezoelectric ultrasound transducers, IEEE T. Ultrason. Ferr., 58 (2011) 2699-2707.

[5] P. Liu, H. Sohn, Numerical simulation of damage detection using laser-generated ultrasound, Ultrasonics, 69 (2016) 248-258.

[6] L. Qiu, B. Liu, S. Yuan, Z. Su, Impact imaging of aircraft composite structure based on a model-independent spatial-wavenumber filter, Ultrasonics, 64 (2016) 10-24.

[7] Z. Liu, Q. Xu, Y. Gong, C. He, B. Wu, A new multichannel time reversal focusing method for circumferential Lamb waves and its applications for defect detection in thick-walled pipe with large-diameter, Ultrasonics, 54 (2014) 1967-1976.

[8] L. Yu, V. Giurgiutiu, *In situ* 2-D piezoelectric wafer active sensors arrays for guided wave damage detection, Ultrasonics, 48 (2008) 117-134.

[9] Z. Su, L. Ye, Y. Lu, Guided Lamb waves for identification of damage in composite structures: A review, J. Sound. Vib., 295 (2006) 753-780.

[10] W. Ostachowicz, P. Kudela, P. Malinowski, T. Wandowski, Damage localisation in plate-like structures based on PZT sensors, Mech. Syst. Signal. Pr., 23 (2009) 1805-1829.

[11] V. Giurgiutiu, Tuned Lamb wave excitation and detection with piezoelectric wafer active sensors for structural health monitoring, J. Intel. Mat. Syst. Str., 16 (2005) 291-305.

[12] D.A. Hutchins, D. Billson, R. Bradley, K. Ho, Structural health monitoring using polymer-based capacitive micromachined ultrasonic transducers (CMUTs), Ultrasonics, 51 (2011) 870-877.

[13] T.S. Jang, S.S. Lee, Y.G. Kim, Surface-bonded fiber optic Sagnac sensors for ultrasound detection, Ultrasonics, 42 (2004) 837-841.

[14] J. Park, Y. Je, H. Lee, W. Moon, Design of an ultrasonic sensor for measuring distance and detecting obstacles, Ultrasonics, 50 (2010) 340-346.

[15] E. Frankforter, B. Lin, V. Giurgiutiu, Characterization and optimization of an ultrasonic piezo-optical ring sensor, Smart Mater. Struct., 25 (2016) 045006.

[16] B. Ren, C.J. Lissenden, PVDF Multielement Lamb Wave Sensor for Structural Health Monitoring, IEEE T. Ultrason. Ferr., 63 (2016) 178-185.

[17] X.P. Qing, S. Beard, S.B. Shen, S. Banerjee, I. Bradley, M.M. Salama, F.-K. Chang, Development of a real-time active pipeline integrity detection system, Smart Mater. Struct., 18 (2009) 115010.

[18] A.B. Thien, H.C. Chiamori, J.T. Ching, J.R. Wait, G. Park, The use of macro-fibre composites for pipeline structural health assessment, Struct. Control. Health Monit., 15 (2008) 43-63.

[19] D.N. Alleyne, B. Pavlakovic, M.J.S. Lowe, P. Cawley, Rapid, long range inspection of chemical plant pipework using guided waves, AIP Conf. Proc., 557 (2001) 180-187.

[20] P.-M. Lam, K.-T. Lau, H.-Y. Ling, Z. Su, H.-Y. Tam, Acousto-ultrasonic sensing for delaminated GFRP composites using an embedded FBG sensor, Opt. Lasers Eng.., 47 (2009) 1049-1055.

[21] F. Li, Z. Su, L. Ye, G. Meng, A correlation filtering-based matching pursuit (CF-MP) for damage identification using Lamb waves, Smart Mater. Struct., 15 (2006) 1585-1594.

[22] Z. Su, C. Zhou, M. Hong, L. Cheng, Q. Wang, X. Qing, Acousto-ultrasonics-based fatigue damage characterization: Linear versus nonlinear signal features, Mech. Syst. Signal Process., 45 (2014) 225-239.

[23] L. Gao, E.T. Thostenson, Z. Zhang, T.-W. Chou, Sensing of damage mechanisms in fiber-reinforced composites under cyclic loading using carbon nanotubes, Adv. Funct. Mater., 19 (2009) 123-130.

[24] K.J. Kim, W.-R. Yu, J.S. Lee, L. Gao, E.T. Thostenson, T.-W. Chou, J.-H. Byun, Damage characterization of 3D braided composites using carbon nanotube-based *in situ* sensing, Compos. Part A-Appl. S., 41 (2010) 1531-1537.

[25] J. Sebastian, N. Schehl, M. Bouchard, M. Boehle, L. Li, A. Lagounov, K. Lafdi, Health monitoring of structural composites with embedded carbon nanotube coated glass fiber sensors, Carbon, 66 (2014) 191-200.

[26] E.T. Thostenson, T.W. Chou, Carbon nanotube networks: sensing of distributed strain and damage for life prediction and self healing, Adv. Mater., 18 (2006) 2837-2841.

[27] Alamusi, N. Hu, H. Fukunaga, S. Atobe, Y. Liu, J. Li, Piezoresistive strain sensors made from carbon nanotubes based polymer nanocomposites, Sensors, 11 (2011) 10691-10723.

[28] Z. Zeng, M. Liu, H. Xu, W. Liu, Y. Liao, H. Jin, L. Zhou, Z. Zhang, Z. Su, A coatable, light-weight, fast-response nanocomposite sensor for the *in situ* acquisition of dynamic elastic disturbance: from structural vibration to ultrasonic waves, Smart Mater. Struct., 25 (2016) 065005.

[29] A. Ferrreira, J.G. Rocha, A. Ansón-Casaos, M.T. Martínez, F. Vaz, S. Lanceros-Mendez, Electromechanical performance of poly(vinylidene fluoride)/carbon nanotube composites for strain sensor applications, Sensor. Actuat. A-phys., 178 (2012) 10-16.

[30] G. Georgousis, C. Pandis, A. Kalamiotis, P. Georgiopoulos, A. Kyritsis, E. Kontou, P. Pissis, M. Micusik, K. Czanikova, J. Kulicek, M. Omastova, Strain sensing in polymer/carbon nanotube composites by electrical resistance measurement, Compos. Part. B Eng., 68 (2015) 162-169.

[31] N. Hu, T. Itoi, T. Akagi, T. Kojima, J. Xue, C. Yan, S. Atobe, H. Fukunaga, W. Yuan, H. Ning, Surina, Y. Liu, Alamusi, Ultrasensitive strain sensors made from metal-coated carbon nanofiller/epoxy composites, Carbon, 51 (2013) 202-212.

[32] N. Hu, Y. Karube, M. Arai, T. Watanabe, C. Yan, Y. Li, Y. Liu, H. Fukunaga, Investigation on sensitivity of a polymer/carbon nanotube composite strain sensor, Carbon, 48 (2010) 680-687.

[33] N. Hu, Y. Karube, C. Yan, Z. Masuda, H. Fukunaga, Tunneling effect in a polymer/carbon nanotube nanocomposite strain sensor, Acta Mater., 56 (2008) 2929-2936.

[34] S.-H. Hwang, H.W. Park, Y.-B. Park, Piezoresistive behavior and multi-directional strain sensing ability of carbon nanotube–graphene nanoplatelet hybrid sheets, Smart Mater.

Struct., 22 (2013) 015013.

[35] W. Li, J. Yuan, A. Dichiara, Y. Lin, J. Bai, The use of vertically aligned carbon nanotubes grown on SiC for *in situ* sensing of elastic and plastic deformation in electrically percolative epoxy composites, Carbon, 50 (2012) 4298-4301.

[36] A.I. Oliva-Avilés, F. Avilés, V. Sosa, Electrical and piezoresistive properties of multi-walled carbon nanotube/polymer composite films aligned by an electric field, Carbon, 49 (2011) 2989-2997.

[37] K. Parmar, M. Mahmoodi, C. Park, S.S. Park, Effect of CNT alignment on the strain sensing capability of carbon nanotube composites, Smart Mater. Struct., 22 (2013) 075006.

[38] M. Penza, P. Aversa, G. Cassano, W. Wlodarski, K. Kalantarzadeh, Layered SAW gas sensor with single-walled carbon nanotube-based nanocomposite coating, Sensor Actuat. B Chem., 127 (2007) 168-178.

[39] S. Sivaramakrishnan, R. Rajamani, C.S. Smith, K.A. McGee, K.R. Mann, N. Yamashita, Carbon nanotube-coated surface acoustic wave sensor for carbon dioxide sensing, Sensor Actuat. B Chem., 132 (2008) 296-304.

[40] H. Yazdani, K. Hatami, E. Khosravi, K. Harper, B.P. Grady, Strain-sensitive conductivity of carbon black-filled PVC composites subjected to cyclic loading, Carbon, 79 (2014) 393-405.

[41] M.H. Al-Saleh, U. Sundararaj, A review of vapor grown carbon nanofiber/polymer conductive composites, Carbon, 47 (2009) 2-22.

[42] G. Tibbetts, M. Lake, K. Strong, B. Rice, A review of the fabrication and properties of

vapor-grown carbon nanofiber/polymer composites, Compos. Sci. Technol., 67 (2007) 1709-1718.

[43] S.-H. Bae, Y. Lee, B.K. Sharma, H.-J. Lee, J.-H. Kim, J.-H. Ahn, Graphene-based transparent strain sensor, Carbon, 51 (2013) 236-242.

[44] Y. Wang, L. Wang, T. Yang, X. Li, X. Zang, M. Zhu, K. Wang, D. Wu, H. Zhu, Wearable and highly sensitive graphene strain sensors for human motion monitoring, Adv. Funct. Mater., 24 (2014) 4666-4670.

[45] M. Castro, J. Lu, S. Bruzaud, B. Kumar, J.-F. Feller, Carbon nanotubes/poly(ε-caprolactone) composite vapour sensors, Carbon, 47 (2009) 1930-1942.

[46] J. Lu, B. Kumar, M. Castro, J.-F. Feller, Vapour sensing with conductive polymer nanocomposites (CPC): Polycarbonate-carbon nanotubes transducers with hierarchical structure processed by spray layer by layer, Sensor Actuat. B Chem., 140 (2009) 451-460.

[47] F. Su, M. Miao, Effect of MWCNT dimension on the electrical percolation and mechanical properties of poly(vinylidenefluoride-hexafluoropropylene) based nanocomposites, Synthetic Met., 191 (2014) 99-103.

[48] G.B. Santoni, L. Yu, B. Xu, V. Giurgiutiu, Lamb wave-mode tuning of piezoelectric wafer active sensors for structural health monitoring, J. Vib. Acoust., 129 (2007) 752-762.

[49] L. Qiu, M. Liu, X. Qing, S. Yuan, A quantitative multidamage monitoring method for large-scale complex composite, Struct. Health. Monit., 12 (2013) 183-196.